Talanta 132 (2015) 215–221

Contents lists available at ScienceDirect

Talanta

journal homepage: www.elsevier.com/locate/talanta

A carboxylated graphene and aptamer nanocomposite-based aptasensor for sensitive and specific detection of hemin

Ling Gao, Yinghong Xiao *, Yanping Wang, Xue Chen, Bo Zhou, Xiaodi Yang **

Jiangsu Key Laboratory of New Power Batteries, Jiangsu Collaborative Innovation Center of Biomedical Functional Materials, College of Chemistry and Material Science, Nanjing Normal University, Nanjing 210097, China

ARTICLE INFO

Article history:
Received 12 May 2014
Received in revised form
3 September 2014
Accepted 7 September 2014
Available online 16 September 2014

Keywords:
Carboxylated grapheme
Functionalized electrode
Nanocomposite aptasensor

ABSTRACT

A unique nanocomposite was crafted by grafting hemin-binding-aptamer (HBA) onto carboxylated graphene (COO-GR). Infrared spectroscopy, Raman spectroscopy and diffuse reflectance spectra suggested that –NHCO– covalent bonds were formed between HBA and COO-GR. The resulting COO-GR/HBA functionalized electrode was used as a novel label-free biosensor. The square wave voltammetry was employed to realize the selective and specific detection of hemin. The obtained aptasensor possessed excellent performance with a detection limit of 0.64 nmol L^{-1} ($S/N=3$) and a linear range from 1 to 150 nmol L^{-1}. Moreover, COO-GR was shown to be a promising candidate in making aptasensors, carrying advantages over graphene in terms of the simplicity of sensor preparation and the reduction of background noise.

1. Introduction

Aptamers are capable of binding specific target molecules with high selectivity and affinity. Due to the ease of production in vitro, wide target range, modification ease, reversible thermal denaturation and unlimited shelf life, aptamers are believed to be excellent alternatives to antibodies for recognizing proteins [1–3]. During the past decades, aptamers have been widely studied and exploited for disease diagnoses, biological assay and aptamer-based sensors [4–7]. To monitor the aptamer–target molecule interactions, a label-free method for aptamer-based analysis would make the process simple and easy. However, the sensitivity and electrochemical stability of aptamer-modified electrodes are usually unsatisfactory. To this end, aptamers have to be immobilized onto a variety of solid substrates with large specific surface areas to improve their sensing performances [8–12].

Graphene is a two-dimensional (2D) sheet of covalently bonded carbon atoms, with the highest surface-to-volume ratio, excellent electrical and mechanical performance and thermal stability [13–15]. Graphene and its derivatives offer possibilities for highly sensitive detection with the advantageous large specific surface areas, and have been used as substrates in electroanalytical chemistry [16–18].

Hemin, a well-known natural porphyrinatoiron complex, is an important compound and has been applied in pharmacy, environmental science, food industry and bioscience and technology [19–21]. While there are many studies on the high electrocatalytic activity of hemin for peroxidation reactions in analytical applications as well as in the application of determination of H_2O_2 and related compounds [22–25], studies regarding the detection of hemin as a target are relatively scarce. In this context, it is of great importance to develop a new method for the determination of hemin with high sensitivity and selectivity.

Herein, we report a novel method to develop a highly sensitive label-free electrochemical aptasensor for hemin detection. The proposed method is based on a nanocomposite composed of hemin-binding-aptamer (HBA) and carboxylated graphene (COO-GR), as shown in Scheme 1. In particular, HBA and COO-GR composite was prepared by simply mixing the aqueous solutions of both components. The resulting nanocomposite was immobilized on the surface of glassy carbon electrode (GCE) to construct a sensing platform. The introduction of nanomaterials greatly improved the specific surface area and electrochemical stability of the aptamer-modified electrode. As a result, the modified electrode exhibited high performances on electrochemical sensing of hemin. We note that instead of graphene, COO-GR was employed due to its better dispersibility in water and ease of preparation of the COO-GR/HBA nanocomposite.

2. Experimental

2.1. Materials and reagents

HBA was purchased from Bioneer Trade Co., Ltd. (Shanghai, China). The sequence of HBA is 5′-NH_2-GTG GGT AGG GCG GGT

* Corresponding author. Tel./fax: +86 25 85891536.
** Corresponding author. Tel.: +86 25 83598648; fax: +86 25 83598280.
E-mail addresses: yhxiao@njnu.edu.cn (Y. Xiao), yangxiaodi@njnu.edu.cn (X. Yang).

http://dx.doi.org/10.1016/j.talanta.2014.09.010
0039-9140/

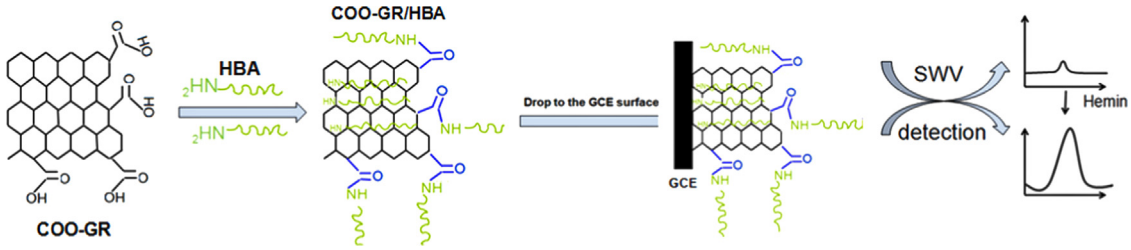

Scheme 1. Schematic diagram for the preparation of the aptasensor based on COO-GR/HBA nanocomposite for sensitive hemin detection.

TGG-3′ and complementary oligonucleotide sequence is 5′-NH_2-CAC ACA CAC ACA CAC ACA CAC-3′. Hemin was obtained from RED Chemical Co., Ltd. (Shanghai, China). Human serum was supplied by Nanjing Maternity and Child Health Care Hospital (Nanjing, China). COO-GR was purchased from Nanjing XFNANO Materials Tech Co., Ltd. (Nanjing, China). 1-Ethyl-3-(3-dimethy-aminopropyl) carbodiimide hydrochloride (EDC) and N-hydroxysuccinimide (NHS) were purchased from Sigma-Aldrich (Spain). All other chemicals were of analytical grade and purchased from Sigma-Aldrich (Netherlands). Double-distilled water (DDW) was used in making all aqueous solutions.

2.2. Characterizations

Zeta Potential was determined using Zetasizer Nano 90 (Malvern, Britain). The samples were dispersed in water with sonication at ambient temperature. Cyclic voltammetry (CV), differential pulse voltammetry (DPV), electrochemical impedance spectroscopy (EIS) and square wave voltammetry (SWV) were conducted using CHI660B electrochemical analyzer (CH Instruments, Chenhua Inc., Shanghai, China). A three-electrode system was employed consisting of a modified GCE working electrode, a platinum wire counter electrode and a Ag/AgCl (saturated with KCl) reference electrode. Fourier transform infrared (FTIR) spectroscopy was recorded with a Cary 5000 spectrophotometer (Varian Co., USA). 2 mg mL^{-1} COO-GR and 10 μmol L^{-1} HBA were mixed at a volume ratio of 4:1. An aliquot of the mixture (COO-GR/HBA), 2 mg mL^{-1} COO-GR and 10 μmol L^{-1} HBA were dropped on the cleaned KBr disks, respectively and dried under an Infrared lamp. Diffuse reflectance spectra were obtained with the same Cary 5000 spectrophotometer and samples were dropped on the cleaned quartz plates for characterization. Raman spectra were measured on a LabRAM HR800 confocal spectrometer (Jobin Yvon, France), with 514.5 nm Ar laser excitation.

2.3. Fabrication of COO-GR modified electrode

GCE was sequentially polished to a mirror finish with 0.3 μm and 0.5 μm alumina slurry and washed with absolute alcohol followed by rinsing thoroughly with DDW. Finally, the polished electrode was allowed to dry at room temperature after ultrasonication cleaning for 5 min in DDW. 10 μL of 1.6 mg mL^{-1} COO-GR was coated on a cleaned GCE surface and dried in air. The electrode was rinsed thoroughly with 0.1 mol L^{-1} phosphate buffer solution (PBS, pH 7.4) and DDW before application.

2.4. Fabrication of COO-GR/HBA modified electrode

2 mg mL^{-1} COO-GR and 10 μmol L^{-1} HBA were mixed at a volume ratio of 4:1. 10 μL of the mixture (COO-GR/HBA) was blended with 2 μL chitosan adhesive, coated on the cleaned GCE surface and dried in air. The electrode was rinsed thoroughly with 0.1 mol L^{-1} PBS (pH 7.4) and DDW before application.

2.5. Fabrication of graphene/HBA modified electrode

Graphene/HBA modified electrode was fabricated for comparison. Graphene coated GCE was prepared using the same method reported in our previous study [4]. The thus obtained graphene–GCE was activated with 0.5 mL of 0.1 mol L^{-1} PBS containing 10 mmol L^{-1} EDC and 10 mmol L^{-1} NHS for 16 h. Subsequently, the electrode was immersed in 1 mL of 1 μmol L^{-1} HBA containing 0.1 mol L^{-1} NaCl and 4 mol L^{-1} EDTA for at least 24 h at ambient temperature. Finally, the electrode was rinsed with copious DDW to remove any unfixed aptamer molecules.

2.6. Electrochemical measurements

The electrochemical performances of the modified electrodes were investigated by CV, DPV and EIS in a 0.1 mol L^{-1} PBS solution (pH 7.4) containing 10 mmol L^{-1} $[Fe(CN)_6]^{3-/4-}$ and 0.1 mol L^{-1} KCl. CV was swept within potential scanning range from 0.6 to −0.1 V with different scan rates. DPV was conducted with pulse amplitude of 0.05 V, pulse width of 0.05 s and pulse period of 0.2 s. For EIS measurements, an AC sinusoid of 5.0 mV in amplitude was applied as input signal, with the DC potential set to 0.28 V over a wide frequency range from 10^0 to 10^5 Hz.

2.7. Detection of target hemin

Fresh hemin solutions were prepared prior to each experiment by dissolving hemin with a few microliters of 0.1 mol L^{-1} NaOH and subsequent addition of PBS to the requested concentrations. Highly pure N_2 was bubbled through the cell solution for about 20 min prior to each experiment. Detection of hemin was carried out by immersing the COO-GR/HBA modified electrode into a 0.1 mol L^{-1} PBS containing hemin with different concentrations. The resulting change of peak current upon the binding of HBA with hemin was monitored using SWV. SWV was performed with potential scanning from 0.8 to −0.1 V with quiet time of 120 s, scan increment of 4 mV, amplitude of 25 mV and frequency of 15 Hz.

3. Results and discussion

3.1. Chemical structure of COO-GR/HBA

FTIR, diffusion reflectance spectra and Raman spectroscopy were employed to examine the covalent bond formation between HBA and –COOH. Fig. 1A (a) exhibits the characteristic absorption peaks of COO-GR. A broad band ranging from 3600 to 3250 cm^{-1} indicates the presence of –OH groups. –COOH groups in COO-GR is evidenced by the C=O stretching vibration at 1725 cm^{-1}, the –COO asymmetric stretching shoulder peak at 1570 cm^{-1}, and –COO symmetric stretching vibration at 1415 cm^{-1}. A C=C aromatic ring stretching vibration is present at 1635 cm^{-1} [26]. Spectrum of HBA displays a broad band around 3166 cm^{-1}

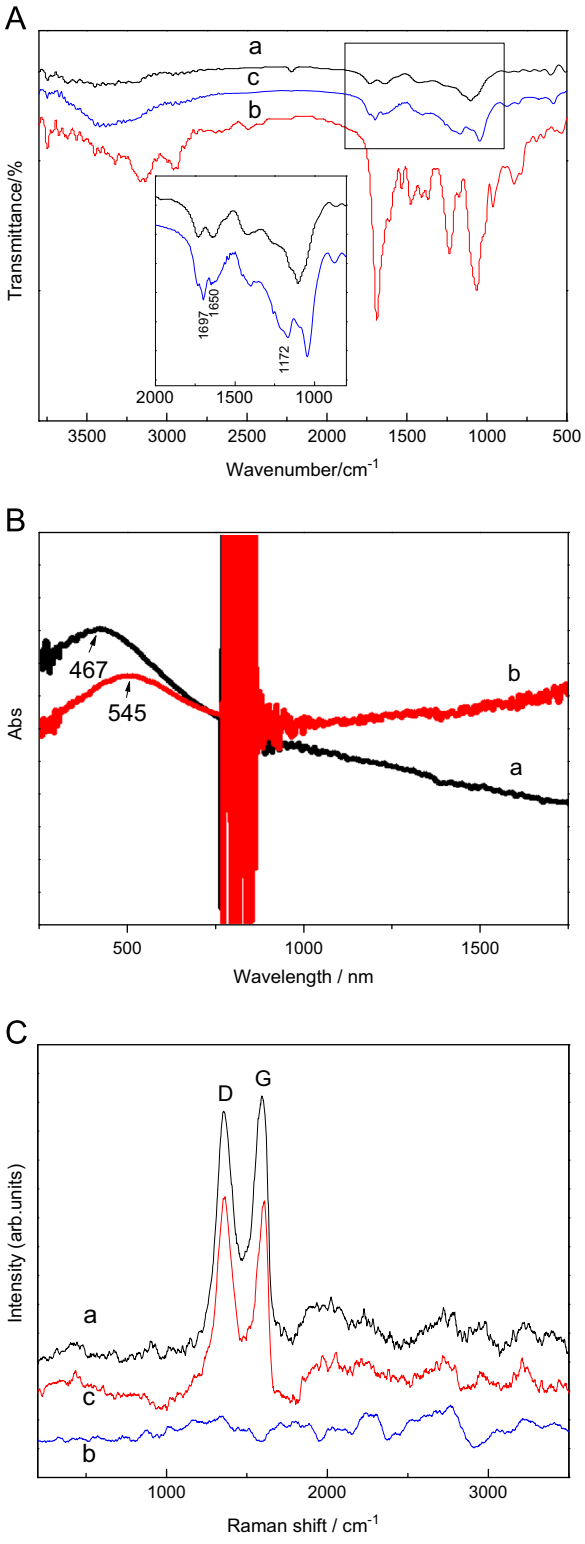

Fig. 1. (A) FTIR of COO-GR (a), HBA (b), and COO-GR/HBA (c). (B) Diffusion reflectance spectra of COO-GR (a) and COO-GR/HBA (b). (C) Raman spectra of COO-GR (a), HBA (b), and COO-GR/HBA (c).

of –N–H stretching vibration, an absorption peak of C=O at 1685 cm^{-1}, a stretching peak at 1228 cm^{-1} of –CN and a dissymmetric stretching vibration of phosphate radicals at 1066 cm^{-1} (b). In the spectrum of the COO-GR/HBA composite, the increase in the intensity of the band around 3400 cm^{-1} is assigned to the presence of –OH groups in COO-GR and –N–H in HBA. The new absorption peaks at 1697 cm^{-1}, 1650 cm^{-1} and 1172 cm^{-1} are attributed to the C=O vibration in –NHCO–, in-plane bending mode of –N–H, and –CN vibration, respectively (c). Diffuse reflectance also reveals the covalent binding of COO-GR and HBA. The noise around 800 nm was caused by the change of the detector from UV to visible light. The featured change of C=O absorbance band from 467 nm in COO-GR to 545 nm in COO-GR/HBA indicates a conversion from –COOH to –NHCO– (B). Raman spectroscopy is a powerful tool to characterize the bonding, ordering, and crystallite size of carbon materials. It is well known that the Raman band at ~1590 cm^{-1} (the G-band) is due to the in-plane phonon modes of graphene, showing the sp^2 bonding. The band around ~1360 cm^{-1} is due to disorder in the graphene layers caused by the presence of sp^3 bonding (the D-band). As can be seen in Fig. 1C, COO-GR also exhibits the two bands with the G band being higher (a), which is in agreement with the previous report [26]. It is reasonable that HBA does not show any featured bands in Raman spectroscopy (b). After binding with HBA, however, the D band of the COO-GR/HBA becomes prominent (c). The HBA molecules decorated on COO-GR cause the sp^2 delocalization due to their strong negativity. sp^2 structures close to the decorated points convert to sp^3 structures, leading to the increase of the D/G intensity ratio for COO-GR/HBA.

3.2. Comparison of COO-GR and graphene for the construction of aptasensors

To clearly show the advantage of COO-GR over graphene in this study, both COO-GR/HBA and graphene/HBA modified electrodes were prepared and characterized as follows. As shown in Fig. 2A, DPV reveals that the peak current of COO-GR/HBA increases compared with COO-GR–GCE; while the peak current of graphene/HBA decreases in comparison with graphene–GCE. In addition, both graphene and graphene/HBA modified electrodes present high background current while the COO-GR and COO-GR/HBA modified electrodes nearly have no background noise, indicating a higher signal to noise ratio (S/N) of the COO-GR based electrodes. EIS measurements (Fig. 2B) suggest that after binding with HBA the charge transfer resistance (R_{et}) of graphene increases by 196 Ω (from a to b) while the R_{et} of COO-GR decreases by 358 Ω (from c to d). The phenomenon is reasonable as graphene is known for its excellent electrical conductivity and immobilization of HBA on graphene will form an organic layer, thus unambiguously increases the surface resistance. As for COO-GR, the existence of carboxylic groups anchoring at the edges of graphene molecules destroys the sp^2 hybridization conjugation of the backbone, thereby inhibiting the electron transfer and resulting in a poor conductivity as well as a high impedance of the coated electrode. Interestingly, the R_{et} of COO-GR/HBA greatly decreases instead. We assume that the R_{et} at electrode/electrolyte interface is determined by two factors: (1) the electrical conductivity of the coating, and (2) the charges of the coating surface. A possible explanation to this phenomenon is that after binding with HBA, –NH_2 groups decorated on HBA are covalently bonded with –COOH to form strong amide bonds, leading to a change in charges of the resulting surface. This assumption is verified by Zeta potential measurements. In a solution with pH=7.4, the Zeta potentials of COO-GR and COO-GR/HBA are −7.65 mV and −0.905 mV, respectively. Another advantage of the current strategy is that the preparation of COO-GR/HBA is relatively simple in comparison with that of graphene/HBA due to the better water solubility of COO-GR (see Section 2).

3.3. Electrochemical characterization of the modified electrodes

Electrochemical properties of the modified electrodes investigated by CV, DPV and EIS are shown in Fig. 3. Compared with the

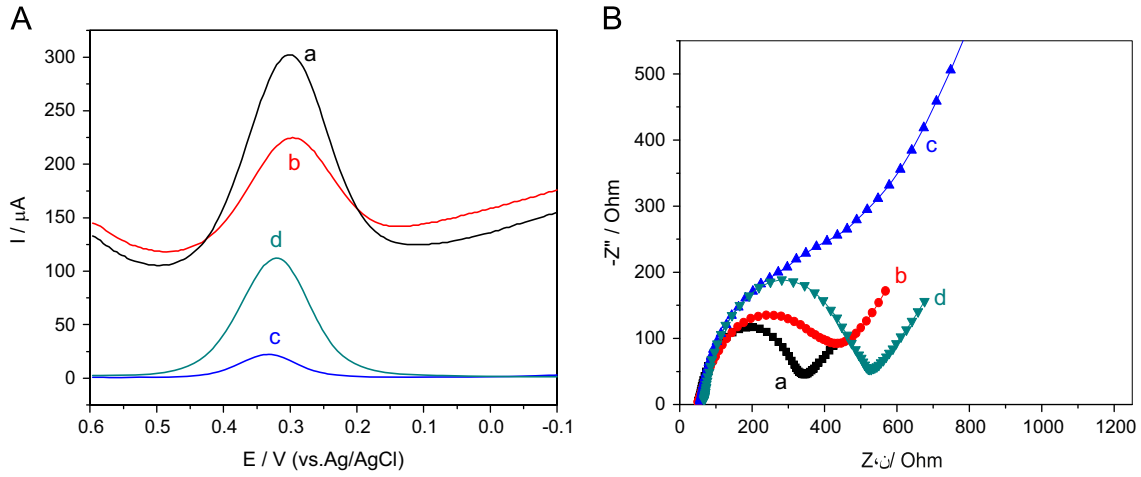

Fig. 2. DPV (A) and EIS (B) of GR (a), GR/HBA (b), COO-GR (c) and COO-GR/HBA electrode (d) in 0.1 mol L^{-1} PBS (pH 7.4) containing 10 mmol L^{-1} $[Fe(CN)_6]^{3-/4-}$ and 0.1 mol L^{-1} KCl.

bare GCE, the COO-GR modified electrode exhibits relatively poor electrochemical performance. In particular, (1) the enclosed area in CV largely decreases, indicating its low charge capability; (2) the peak current in DPV decreases, implying its decreased conductivity; and (3) the R_{et} greatly increases. As discussed above, the existence of carboxylic groups anchoring at the edges of graphene molecules causes the destruction of sp^2 hybridization conjugation of the carbon backbone, leading to poor conductivity of the COO-GR coated electrode. However, after binding with HBA, the electrochemical performance improves as clearly evidenced by the enlarged enclosed area in CV, the increased peak current in DPV, and the decreased R_{et} in EIS. This is due to the fact that $-NH_2$ groups decorated on HBA are covalently bonded with –COOH to form strong amide bonds, and thus the amount of carboxyl groups on the electrode surface is greatly reduced, leading to less negative charges on the surface as confirmed by Zeta potential. The variation of the surface charges has a key influence on the R_{et} at the electrode/electrolyte interface.

3.4. Relationship between peak current and scan rate of CV

To understand the redox kinetics of the functionalized electrode, CV measurements of the COO-GR/HBA electrode at various scan rates were performed. The resulting plots are shown in Fig. 4A. Theoretically, when electron transfer at the interface is fast enough and redox reactions are totally reversible, the difference of peak current (ΔE_p) will remain constant and will not change with scan rate. However, in our study we note that with increasing scan rate from 10 to 200 mV s^{-1}, the anodic peak shifts to more positive positions, while the cathodic peak shifts to more negative positions. As a result, ΔE_p changes from 20 to 80 mV. Meanwhile, both anodic and cathodic peak currents increase with increasing scan rate. Fig. 4B displays the relationship between peak current (I_{pa} and I_{pc}) and square root of the scan rate $v^{1/2}$. The linear relationship is expressed by $I_{pa} = -3.807 \times 10^{-5} v^{1/2} + 1.341 \times 10^{-5}$ ($R^2_{pa} = 0.9939$) and $I_{pc} = 3.414 \times 10^{-5} v^{1/2} - 1.307 \times 10^{-5}$ ($R^2_{pc} = 0.9920$), respectively. The results reveal a quazi-reversible electrochemical kinetics and diffusion-controlled process of the electrochemical reaction at the electrode surface.

3.5. Quantitative detection of hemin

As it is well known, COO-GR on its own can form molecular π–π conjugations with hemin molecules. In the meantime, COO-GR exhibits good electrocatalytic reducibility towards hemin. Thus, a COO-GR coated electrode was applied to directly detect hemin with SWV. Interestingly, the current peaks appear at 0.22 V and the peak current varies with hemin concentrations from 0.1 to 5 μmol L^{-1} (Fig. 5), indicating the responsibility of the COO-GR coated electrode to hemin. It is reasonable because more hemin molecules will be immobilized on to COO-GR when its concentration gets higher. However, no linear relationship was found between peak currents and hemin concentrations, which hinders the application of COO-GR modified electrodes in the quantitative detection of hemin.

To explore an ideal approach for quantitatively detect hemin, HBA was immobilized onto the COO-GR coated electrode to yield an aptasensor. Clearly, when the aptasensor was incubated in hemin solution, the peak current at 0.22 V in SWV increased with increasing hemin concentration, a same phenomenon observed for the COO-GR coated electrode. When the concentration of the hemin solution increases, more hemin molecules are immobilized on the electrode surface due to the specific recognition of HBA to hemin, leading to an increased peak current (Fig. 6A). The different phenomenon from that of the COO-GR coated electrode is as follows: there is a linear relationship between the peak currents and hemin concentrations from 1 to 150 nmol L^{-1}, after which the current reaches a plateau, implying the saturation of hemin on the electrode surface (Fig. 6B). The regression equation is $I = 0.4685c + 30.9130$, with a linear coefficient of $R^2 = 0.9940$ and a detection limit of 0.64 nmol L^{-1} ($S/N = 3$). The resulting aptasensor exhibits better performance than the reported nano-ZnO-carbon paste electrode with a linear range from 3.07×10^{-9} to 3.07×10^{-7} mol L^{-1} and the fluorescence aptasensor with a linear range of 0.31–2.50 μmol L^{-1}. Furthermore, the detection limit of 0.64 nmol L^{-1} is lower than that of the reported electrochemical sensor (1.5×10^{-9} mol L^{-1}) as well as the fluorescence aptasensor (50 nmol L^{-1}) [27,28].

3.6. Specificity of the COO-GR/HBA aptasensor

Specificity is another important performance for aptasensors to accurately detect analytes in real applications. To evaluate the specificity of the fabricated COO-GR/HBA aptasensor to hemin, standard recoveries were determined based on the calibration curve in the presence of serum. We found that the peak currents at 0.22 V are almost the same for the blank solution and the serum solution (Fig. 7). Moreover, when the concentration of hemin in the mixture of serum and hemin was increased, the peak current increased accordingly, in spite of the presence of serum. This

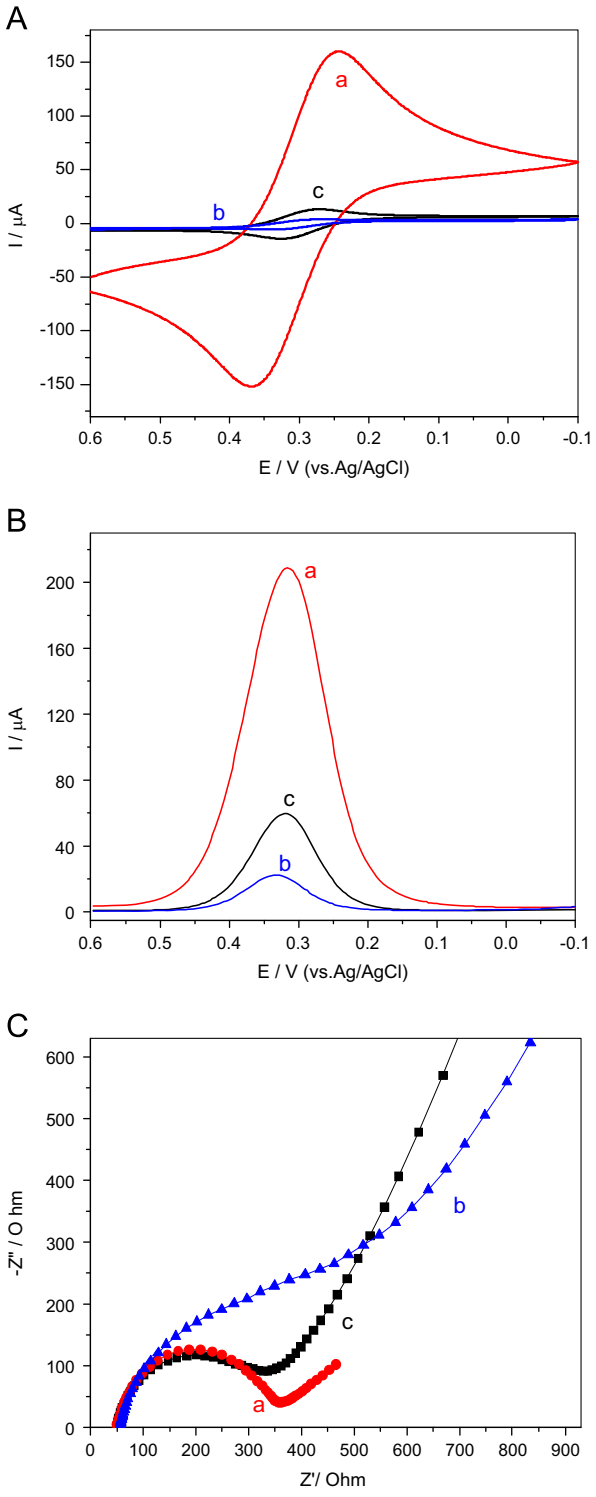

Fig. 3. Electrochemical characterization of bare GCE (a), COO-GR modified electrode (b) and COO-GR/HBA modified electrode (c) in 0.1 mol L^{-1} PBS (pH 7.4) containing 10 mmol L^{-1} $[Fe(CN)_6]^{3-/4-}$ and 0.1 mol L^{-1} KCl. (A) CV, (B) DPV and (C) EIS.

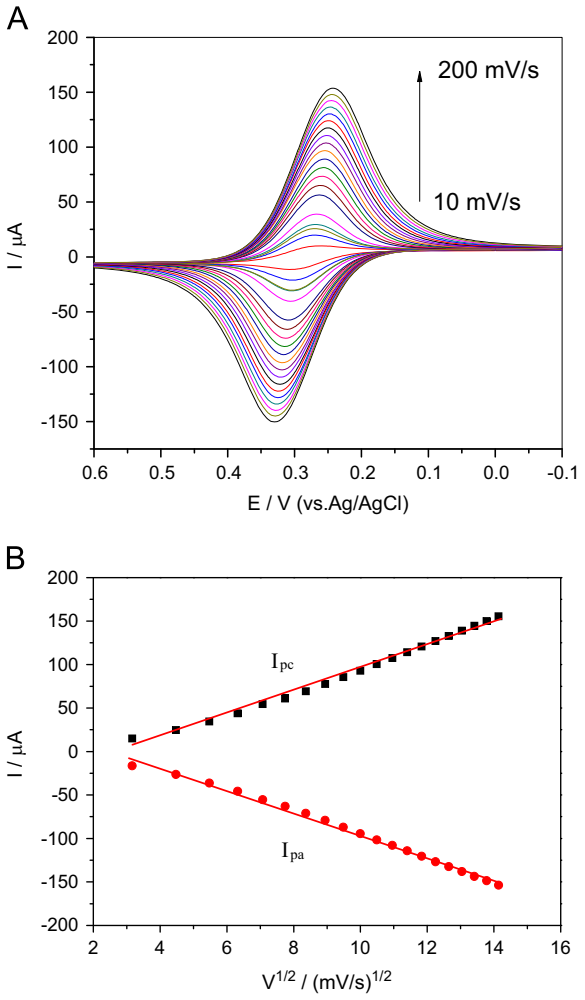

Fig. 4. (A) CVs of the COO-GR/HBA modified electrode with different scan rates in 0.1 mol L^{-1} PBS (pH 7.4) containing 10 mmol L^{-1} $[Fe(CN)_6]^{3-/4-}$ and 0.1 mol L^{-1} KCl. (B) A Randles–Sevik plot of the electrode.

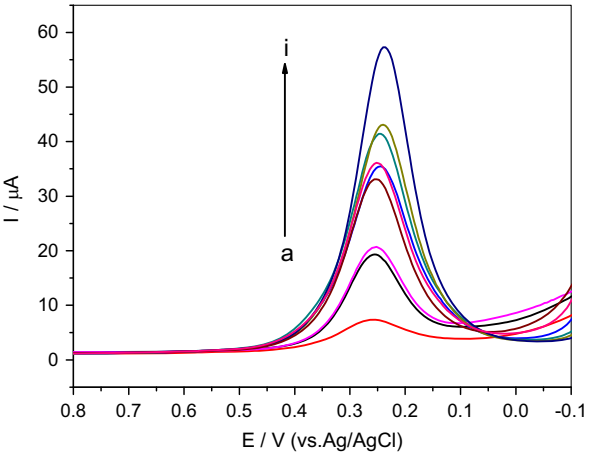

Fig. 5. SWV of the COO-GR coated electrode incubated in hemin with concentrations of 0 (a), 0.1 (b), 0.3 (c), 0.5 (d), 0.7 (e), 2 (f), 3 (g), 4 (h) and 5 μmol L^{-1} (i). Hemin was in 0.1 mol L^{-1} PBS containing 0.1 mol L^{-1} KCl.

demonstrates that the currents change only with hemin concentrations rather than other bio-substances in the mixture. The corresponding data shown in Table 1 indicate that all recoveries turn out to be 97.2–101.9% and fall in the confidence interval of 95–105%, indicating the reliability of the COO-GR/HBA aptasensors in the detection of hemin.

Furthermore, to evaluate the anti-interference property of the fabricated COO-GR/HBA aptasensor, possible interfering species such as K^+, Na^+, Ca^{2+}, NO_3^-, thrombin, adenosine, uridine, cytidine, lysozyme and glucose, which may be present in real samples, were examined in 0.1 mol L^{-1} PBS containing 50 nmol L^{-1} hemin. We found that 50.0-fold of the above species did not show remarkable interference to hemin determination.

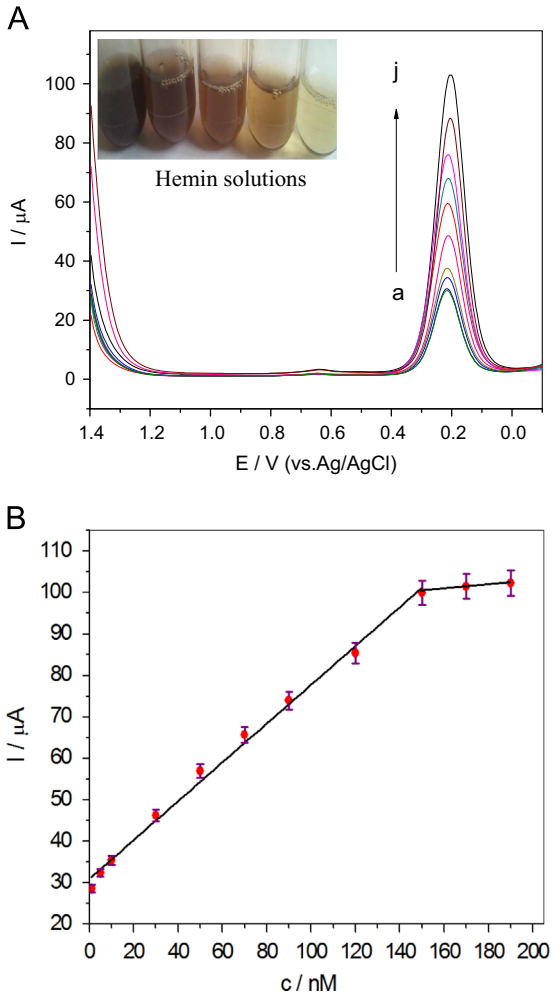

Fig. 6. (A) SWV of the COO-GR/HBA modified electrode incubated in hemin with concentrations of 0 (a), 1 (b), 5 (c), 10 (d), 30 (e), 50 (f), 70 (g), 90 (h), 120 (i) and 150 nmol L^{-1} (j) in 0.1 mol L^{-1} PBS (pH 7.4) containing 0.1 mol L^{-1} KCl. Inset in A is a digital image of hemin solutions with different concentrations. (B) Calibration curve showing the relationship between peak current and hemin concentration. The measurements were repeated 3 times to obtain the standard deviation.

The anti-interference of the COO-GR/HBA aptasensor is acceptable, ensuring its promising application in real sample analysis.

3.7. Analytical performance – repeatability, reproducibility and stability

The repeatability of the sensor response was tested by 10 times successive measurements with the COO-GR/HBA modified electrodes in 0.1 mol L^{-1} PBS containing 50 nmol L^{-1} hemin, giving a satisfying relative standard deviation (RSD) of 1.87%. The reproducibility was examined by six individual determination performed with different COO-GR/HBA modified electrodes in the above solution and the RSD was obtained as 3.69%. Moreover, the proposed aptasensor was stored in 0.1 mol L^{-1} PBS and kept at 4 °C in a fridge. After two weeks, we found that the sensor retained 90.94% of its initial activity. The above results indicated good analytical performance of the proposed aptasensor.

4. Conclusions

Graphene–HBA- and COO-GR–HBA-modified electrodes were crafted and their electrochemical properties were investigated. Although the COO-GR electrode has lower electrical conductivity than that of the graphene electrode, a large number of carboxylic groups in its structure provide active sites for binding with aminated aptamers, HBA. Redox kinetics of the resulting COO-GR–HBA aptasensor is demonstrated to be quazi-reversible and displays a diffusion-controlled process of the electrochemical reaction at the electrode surface. Using SWV as sensing technique, the proposed aptasensor is able to quantitatively detect the analyte of hemin and a detection limit as low as 0.64 nmol L^{-1} can be achieved. Moreover, COO-GR is shown to be a promising candidate in making aptasensors, possessing the advantageous attributes in terms of simplicity of sensor construction and reduction of background noise.

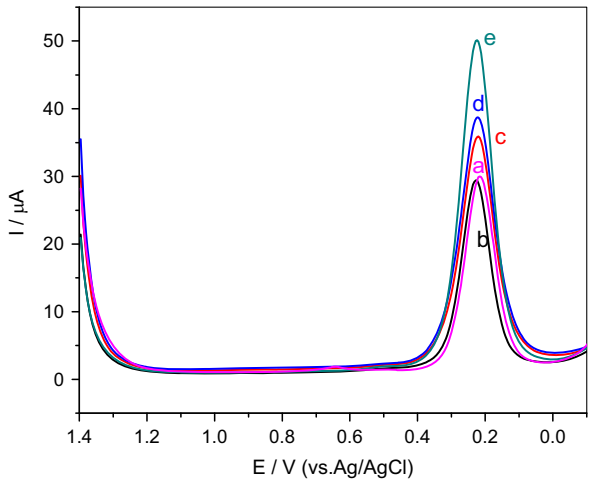

Fig. 7. Specificity analysis of aptasensor tested in blank (a), serum (b) and serum–hemin mixture (c–e). Hemin concentration in serum–hemin mixture is 5 (c), 10 (d) and 35 nmol L^{-1} (e).

Table 1
Standard recovery.

No.	Solution	Concentration of hemin (nmol L^{-1})	Peak current (μA)	Hemin concentration obtained from calibration curve (nmol L^{-1})	Recovery (%)
a	Blank	0	28.12	/	/
b	Serum	0	27.30	/	/
c	Mixture 1 (V_{serum}: V_{hemin}=1:1)	5	33.19	4.86	97.2
d	Mixture 2 (V_{serum}: V_{hemin}=1:2)	10	35.51	9.81	98.1
e	Mixture 3 (V_{serum}: V_{hemin}=1:7)	35	47.63	35.68	101.9

Acknowledgments

The project was funded by the Natural Science Foundation of Jiangsu Province, China (Grant no. BK2012845), the Specialized Research Fund for the Doctoral Program of Higher Education of China (20123219110010), the National Natural Science Foundation of China (21175068), the Foundation of the Jiangsu Education Committee (13KJB150024) and the Priority Academic Program Development of Jiangsu Higher Education Institutions (PAPD).

References

[1] S. Tombelli, M. Minunni, M. Mascini, Biosens. Bioelectron. 20 (2005) 2424.

[2] M. Famulok, J.S. Hartig, G. Mayer, Chem. Rev. 107 (2007) 3715.
[3] P. Zhang, N. Zhao, Z. Zeng, Y. Feng, C.-H. Tung, C.-C. Chang, Y. Zu, Lab. Invest. 89 (2009) 1423.
[4] Y. Wang, Y.H. Xiao, X. Ma, N. Li, X. Yang, Chem. Commun. 48 (2012) 738.
[5] W. Shan, Y. Pan, H. Fang, M. Guo, Z. Nie, Y. Huang, S. Yao, Talanta 126 (2014) 130.
[6] G. Yan, Y. Wang, X. He, K. Wang, J. Liu, Y. Du, Biosens. Bioelectron. 44 (2013) 57.
[7] A. Erdem, G. Congur, Talanta 128 (2014) 428.
[8] X. Jiang, K. Huang, D. Deng, H. Xia, X. Hou, C. Zheng, Trends Anal. Chem. 39 (2012) 38.
[9] G. Jin, L. Lu, X. Gao, M. Li, B. Qiu, Z. Lin, H. Yang, G. Chen, Electrochim. Acta 89 (2013) 13.
[10] M. Pumera, Mater. Today 14 (2011) 308.
[11] X. Dong, Y. Shi, W. Huang, P. Chen, L. Li, J. Adv. Mater. 22 (2010) 1649.
[12] Y.H. Xiao, Y. Wang, M. Wu, X. Ma, X. Yang, J. Electroanal. Chem. 25 (2013) 1922.
[13] K.I. Bolotin, K.J. Sikes, Z. Jiang, M. Klima, G. Fudenberg, J. Hone, P. Kim, H. L. Stormer, Solid State Commun. 146 (2008) 351.
[14] J. Che, L. Shen, Y.H. Xiao, J. Mater. Chem. 20 (2010) 1722.
[15] M.J. Allen, V.C. Tung, R.B. Kaner, Chem. Rev. 110 (2010) 132.
[16] C. Guo, S.R. Ng, S.Y. Khoo, X. Zheng, P. Chen, C.M. Li, ACS Nano 6 (2012) 6944.
[17] M. Pumera, A. Ambrosi, A. Bonanni, E.L.K. Chng, H.L. Poh, Trends Anal. Chem. 29 (2010) 954.
[18] S. Song, Y. Qin, Y. He, Q. Huang, C. Fan, H. Chen, Chem. Soc. Rev. 39 (2010) 4234.
[19] G. Ran, W. Yi, Y. Li, H. Luo, N. Li, Anal. Methods 4 (2012) 2929.
[20] C. Zhou, H. Wang, Y. Chen, C. Chen, Food Sci. Biotechnol. 21 (2012) 669.
[21] J.Y. Wang, Y.T. Lee, P.F. Chang, L.Y. Chau, J. Cell. Physiol. 219 (2009) 617.
[22] M. Zhang, R. Yuan, Y. Chai, S. Chen, X. Zhong, H. Zhong, C. Wang, RSC Adv. 2 (2012) 4639.
[23] S. Xie, Y. Chai, R. Yuan, L. Bai, Y. Yuan, Y. Wang, Anal. Chim. Acta 755 (2012) 46.
[24] A.M. Toader, E. Volanschi, M.F. Lazarescu, V. Lazarescu, Electrochim. Acta 56 (2010) 863.
[25] L. Zhang, J. Zhu, S. Guo, T. Li, J. Li, E. Wang, J. Am. Chem. Soc. 135 (2013) 2403.
[26] K.-W. Park, J. Mater. Chem. A 2 (2014) 4292.
[27] Y. Wang, P. Li, G. Zhan, Chin. J. Appl. Chem. 27 (2010) 1204.
[28] Y. Shi, W. Huang, H. Luo, N. Li, Chem. Commun. 47 (2011) 4676.